Single-atom quantum heat engine based on electromagnetically induced transparency

Jia-Yang Ma, Hong-Zhi Shen, Xiao-Jun Zhang,* and Jin-Hui Wu†
School of Physics and Center for Quantum Sciences, Northeast Normal University, Changchun 130024, China

(Received 5 June 2023; accepted 20 December 2023; published 10 January 2024)

The single-atom version of the quantum heat engine based on electromagnetically induced transparency is theoretically investigated in this paper. In contact with a hot and a cold bath, the atom trapped in an optical cavity is coherently coupled by a coherent field, thus generating photons as output through a process that mimics a heat engine. Using semiclassical theory, we obtain the conditions for the classical gain parameter being positive. Then by taking a full quantum approach, we discuss the statistical property of the generated photons depicted by the photon number distribution and Wigner function, and show that it can be effectively tuned by the coupling field. Investigations on the energy and entropy balances of the heat engine process lead to an interesting result that the power of the engine is simply the energy per time provided by the hot reservoir. The coupling field plays a critical role in supporting the heat-engine process. However, the energy that it provides is all dumped into the cold reservoir. The total energy exchange conforms to the first law of thermodynamics. The efficiency of the engine depends on the temperatures of the two reservoirs and the strength of the coupling field. The entropy change of the heat-engine process suggests that when working far above the threshold of lasing, the efficiency approaches that of its atomic-ensemble-based partner.

DOI: 10.1103/PhysRevA.109.012207

I. INTRODUCTION

Heat engines convert heat or other forms of energy into mechanical work, while quantum heat engines are similar devices but use quantum objects as working materials. It is widely believed that the concept of the quantum heat engine was first introduced in a paper published in 1959, in which Scovil and Schulz-DuBois show that a three-level maser can be regarded as a heat engine (the SSDB heat engine) that takes the Carnot efficiency as its maximum [1]. This paper is also regarded as the starting point of quantum thermodynamics.

Just as studies on the Carnot heat engine led to the establishment of the first and second law of the classical thermodynamics, quantum heat engines offer good models to study the relation between thermodynamics and quantum mechanics [2–4]. The concepts of work, heat, and entropy are extended into the field of quantum optics [5–8]. In the meantime, quantum correlation [9–12], coherence [13–15], quantum interactions [16,17], and statistics [18,19] are explored as new resources to improve the performance of the engine. A quantum heat engine can be operated in cycles [20–22] or in a continuous fashion [23–26]. The example of the former one is the quantum Otto engine [27–29], and the previously mentioned SSDB heat engine belongs to the continuous ones.

Another continuous quantum heat engine that we focus on in this paper is the one first studied by Harris [30]. The model is based on electromagnetically induced transparency (EIT) [31] and is composed of *a group of* ultracold atoms and a coherent laser. When contacting with two heat baths, the engine initiates a series of transitions $|1\rangle \xrightarrow{T_h} |3\rangle \xrightarrow{T_c} |2\rangle \xrightarrow{\omega_c} |3\rangle \xrightarrow{\omega_a} |1\rangle$ [see Fig. 1(a)], leading to the generation of the photons at frequency ω_a. Here T_h is the temperature of the hot reservoir which acts as a source of energy, and T_c is the temperature of the cold reservoir that serves as an entropy tank. Such interaction between the light and the atoms behaves just like an engine, and it has an efficiency that could break the Carnot-engine limit. After proposed in 2016, the engine was demonstrated in laser-cooled ^{85}Rb atoms a year later [32].

In the original model, the generated field (output of the engine) is treated as a classical light, and the features of the system are studied in terms of the linear gain and absorption [30]. As for the quantum characteristic of the generated photons, it can be revealed only using the theory of quantization. Recently the quantum statistics of the single-atom SSDB heat engine have been investigated using the Scully-Lamb approaches [33]. This motivated us to investigate the *single-atom* EIT engine. To the best of our knowledge, the quantum statistics, efficiency, and power of such an engine are not studied yet. We show in this paper that such a single-atom engine behaves quite differently than its semiclassical partner.

Our model is an atom trapped in an optical cavity with the generated photons coupled into a cavity mode. The semiclassical results show that the gain parameter is not a monotonic function of the thermal occupation number of the hot reservoir, since a larger thermal occupation number leads to faster decoherence process and in turn hampers the effect of EIT. When the generated field is quantized, the cases (distinguished by the intensity of coupling field and temperature of hot bath) with the same gain parameter actually have different quantum statistics. Additionally, the properties of the quantum statistics

*zhangxj037@nenu.edu.cn
†jhwu@nenu.edu.cn

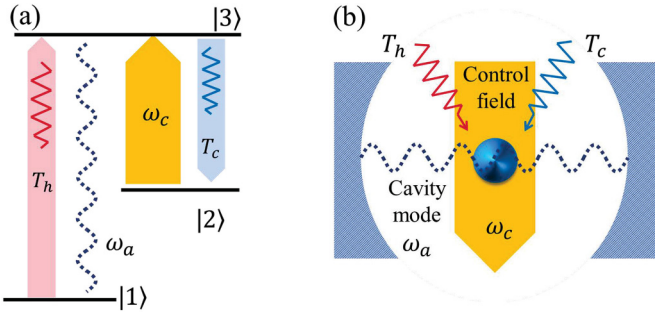

FIG. 1. (a) Single-atom (blue dot) quantum heat engine. Powered by a black-body radiations at temperature T_h and cooled by another at temperature T_c, the atom generates photons in a particular mode at ω_a (dashed wavy line) of an optics cavity, which is regarded as the output of the engine. A strong coupling field at frequency ω_c is used to eliminate the absorption of the generated photons in virtue of EIT. (b) Atomic configuration of the heat engine.

can be controlled by the coupling field. The efficiency of the engine is not a constant as well; it depends on how the engine is powered. In the extreme situation when the engine is far above the lasing threshold, the generated light becomes classical, and the efficiency turns into that of the original engine, which is *not* bounded by the Carnot efficiency.

The remainder of this article is organized as follows. In Sec. II we introduce the model of the engine in detail. The gain and saturation parameters are obtained via a semiclassical analysis. The full quantum calculation is carried out in Sec. III. By solving the master equations, we are able to depict the photon number distribution of the generated photons and its Wiger function as well. The thermodynamics of the engine is investigated in Sec. IV, and we conclude with a summary in Sec. V.

II. MODEL AND CLASSICAL GAIN

Let us consider a single atom interacting with a particular electromagnetic mode of an optical resonator as shown in Fig. 1(b). The atom is assumed to be a three-level system driven by a laser field at frequency ω_c with a Rabi frequency of Ω_c and pumped by two incoherent fields, i.e., black-body radiations with thermal occupation numbers

$$\bar{n}_h = \frac{1}{\exp\left(\frac{\hbar\omega_{31}}{k_b T_h}\right) - 1}, \tag{1a}$$

$$\bar{n}_c = \frac{1}{\exp\left(\frac{\hbar\omega_{32}}{k_b T_c}\right) - 1}, \tag{1b}$$

respectively. Here $\omega_{\alpha\beta}$ is the resonant frequency of the transition $|\alpha\rangle \leftrightarrow |\beta\rangle$, with $\alpha, \beta \in \{1, 2, 3\}$ labeling the atomic energy levels. T_h and T_c are the temperatures of the corresponding black bodies. Similar to the heat engine using that atomic ensemble [30], the atom in the cavity supports the process $|1\rangle \xrightarrow{T_h} |3\rangle \xrightarrow{T_c} |2\rangle \xrightarrow{\omega_c} |3\rangle \xrightarrow{\omega_a} |1\rangle$ as well, and the output photons are generated in a cavity mode at ω_a. In the interaction picture, under the electric-dipole approximation and the rotating-wave approximation, the Hamiltonian of our system is

$$\hat{V} = -\hbar(\Omega_c\hat{\sigma}_{32} + \Omega_c^*\hat{\sigma}_{23} + g_a\hat{a}\hat{\sigma}_{31} + g_a\hat{a}^\dagger\hat{\sigma}_{13}), \tag{2}$$

where $\hat{\sigma}_{\alpha\beta} = |\alpha\rangle\langle\beta|$ is the atomic transition operator, while $\hat{a}$ is the annihilation operator of the cavity mode at frequency ω_a. g_a is the vacuum Rabi frequency of the cavity mode. We assume that the cavity mode and the coupling field resonate with their corresponding transitions, and the dynamics of this cavity-QED system is described by the master equation

$$\frac{\partial}{\partial t}\rho = \frac{i}{\hbar}[\rho, \hat{V}] + \mathscr{L}_h(\rho) + \mathscr{L}_c(\rho) + \mathscr{L}_{\rm cav}(\rho), \tag{3}$$

with

$$\mathscr{L}_h(\rho) = \Gamma_h^+\left(\hat{\sigma}_{31}\rho\hat{\sigma}_{13} - \tfrac{1}{2}\{\hat{\sigma}_{11}, \rho\}\right) + \Gamma_h^-\left(\hat{\sigma}_{13}\rho\hat{\sigma}_{31} - \tfrac{1}{2}\{\hat{\sigma}_{33}, \rho\}\right), \tag{4a}$$

$$\mathscr{L}_c(\rho) = \Gamma_c^+\left(\hat{\sigma}_{32}\rho\hat{\sigma}_{23} - \tfrac{1}{2}\{\hat{\sigma}_{22}, \rho\}\right) + \Gamma_c^-\left(\hat{\sigma}_{23}\rho\hat{\sigma}_{32} - \tfrac{1}{2}\{\hat{\sigma}_{33}, \rho\}\right), \tag{4b}$$

$$\mathscr{L}_{\rm cav}(\rho) = \kappa\left(\hat{a}\rho\hat{a}^\dagger - \tfrac{1}{2}\hat{a}^\dagger\hat{a}\rho - \tfrac{1}{2}\rho\hat{a}^\dagger\hat{a}\right). \tag{4c}$$

Here $\mathscr{L}_h[\rho]$ and $\mathscr{L}_c[\rho]$ describe the contributions from the hot and cold reservoirs, respectively, and

$$\Gamma_h^+ = \Gamma_{31}\bar{n}_h, \quad \Gamma_h^- = \Gamma_{31}(\bar{n}_h + 1),$$
$$\Gamma_c^+ = \Gamma_{32}\bar{n}_c, \quad \Gamma_c^- = \Gamma_{32}(\bar{n}_c + 1).$$

$\Gamma_{\alpha\beta}$ stands for the rate of radiative decay of the transition $|\alpha\rangle \leftrightarrow |\beta\rangle$, and $\mathscr{L}_{\rm cav}[\rho]$ describes the light leaking from the cavity at a rate of κ. Based on Eq. (3), the following equations for the averaged values of the transition operators and the annihilation operator of the cavity mode are obtained:

$$\frac{d\langle\hat{\sigma}_{11}\rangle}{dt} = -\Gamma_h^+\langle\hat{\sigma}_{11}\rangle + \Gamma_h^-\langle\hat{\sigma}_{33}\rangle + ig_a[\langle\hat{\sigma}_{13}\hat{a}^\dagger\rangle - \text{H.c.}], \tag{5a}$$

$$\frac{d\langle\hat{\sigma}_{22}\rangle}{dt} = -\Gamma_c^+\langle\hat{\sigma}_{22}\rangle + \Gamma_c^-\langle\hat{\sigma}_{33}\rangle - i[\Omega_c\langle\hat{\sigma}_{32}\rangle - \text{H.c.}], \tag{5b}$$

$$\frac{d\langle\hat{\sigma}_{12}\rangle}{dt} = -\gamma_{12}\langle\hat{\sigma}_{12}\rangle + i\Omega_c^*\langle\hat{\sigma}_{13}\rangle - ig_a\langle\hat{\sigma}_{32}\hat{a}\rangle, \tag{5c}$$

$$\frac{d\langle\hat{\sigma}_{13}\rangle}{dt} = -\gamma_{13}\langle\hat{\sigma}_{13}\rangle + i\Omega_c\langle\hat{\sigma}_{12}\rangle - ig_a\langle(\hat{\sigma}_{33} - \hat{\sigma}_{11})\hat{a}\rangle, \tag{5d}$$

$$\frac{d\langle\hat{\sigma}_{23}\rangle}{dt} = -\gamma_{23}\langle\hat{\sigma}_{23}\rangle - i\Omega_c\langle\hat{\sigma}_{33} - \hat{\sigma}_{22}\rangle + ig_a\langle\hat{\sigma}_{21}\hat{a}\rangle, \tag{5e}$$

$$\frac{d\langle\hat{a}\rangle}{dt} = -\frac{\kappa}{2}\langle\hat{a}\rangle + ig_a\langle\hat{\sigma}_{13}\rangle. \tag{5f}$$

The decoherence rates in the above equations are $\gamma_{13} = (\Gamma_h^+ + \Gamma_h^- + \Gamma_c^-)/2$, $\gamma_{23} = (\Gamma_h^- + \Gamma_c^- + \Gamma_c^+)/2$, Most importantly

$$\gamma_{12} = \frac{\Gamma_h^+ + \Gamma_c^+}{2} = \frac{\Gamma_{31}\bar{n}_h + \Gamma_{32}\bar{n}_c}{2}. \tag{6}$$

Increasing the thermal occupation number (equivalently the temperature) of either the hot bath or the cold one leads to a larger decoherence rate between ground levels. The

higher temperature of the hot reservoir effectively weakens the phenomenon EIT and increases the absorption on generated photons, and consequently lowers the efficiency of the engine (discussed in Sec. IV).

Instead of seeking exact solutions, we employ the semiclassical approximation, $\langle\hat{\sigma}_{\alpha\beta}\hat{a}\rangle \simeq \langle\hat{\sigma}_{\alpha\beta}\rangle\langle\hat{a}\rangle$ and $\langle\hat{\sigma}_{\alpha\beta}\hat{a}^\dagger\rangle \simeq \langle\hat{\sigma}_{\alpha\beta}\rangle\langle\hat{a}^\dagger\rangle$, to examine the general features of the system. This means that the cavity mode is treated as a classical field, and we define the amplitude of it as $\mathcal{E} := \langle\hat{a}\rangle$. Then Eqs. (5a)–(5e) become the exact equations used in Ref. [30].

Instead of using the perturbation method to find the absorption and emission cross sections that depict the linear response of the atomic system, we manage to solve the equations directly by assuming that atomic system reaches its steady state ($d\langle\hat{\sigma}_{\alpha\beta}\rangle/dt = 0$) quickly due to the fast decay of the atom and $g\mathcal{E} \ll \Omega_c$. Finally we have

$$\frac{d\mathcal{E}}{dt} = -\frac{\kappa}{2}\mathcal{E} + ig_a\langle\hat{\sigma}_{13}\rangle = \frac{1}{2}\left(\frac{G}{1+S|\mathcal{E}|^2} - \kappa\right)\mathcal{E}, \quad (7)$$

with

$$G = 2g^2\frac{|\Omega_c|^2\left[\Gamma_h^+(\Gamma_c^- + \Gamma_h^+) - 2\gamma_{21}\Gamma_h^-\right] + \gamma_{21}\gamma_{32}\Gamma_c^+(\Gamma_h^+ - \Gamma_h^-)}{\left(|\Omega_c|^2 + \gamma_{21}\gamma_{31}\right)\left[2|\Omega_c|^2(\Gamma_h^- + 2\Gamma_h^+) + \gamma_{32}\Gamma_c^+(\Gamma_h^- + \Gamma_h^+) + \gamma_{32}\Gamma_c^-\Gamma_h^+\right]}, \quad (8)$$

$$S = g^2\frac{\gamma_{31}\Gamma_c^+\Gamma_h^- + 2\gamma_{21}\gamma_{32}(\Gamma_c^- + 2\Gamma_c^+) + \gamma_{31}\Gamma_h^+(\Gamma_c^- + \Gamma_c^+) + 2|\Omega_c|^2(4\gamma_{21} + \Gamma_c^- + \Gamma_h^-)}{\left(|\Omega_c|^2 + \gamma_{21}\gamma_{31}\right)\left[2|\Omega_c|^2(\Gamma_h^- + 2\Gamma_h^+) + \gamma_{32}\Gamma_c^+(\Gamma_h^- + \Gamma_h^+) + \gamma_{32}\Gamma_c^-\Gamma_h^+\right]}. \quad (9)$$

Thus $\mathcal{E}$ grows from zero exponentially with respect to time, if G identified as the lasing gain is larger than κ. As it acquires a significant value, the overall amplification effect is further limited by the saturation parameter S. In our system, G and S are determined by the coupling field, thermal occupation numbers of the baths, and the decay rates.

We plot the value of G/κ for different Ω_c and $\bar{n}_h$ in Fig. 2(a). The contour line of $G/\kappa = 1$ corresponds to the lasing threshold of our system for the parameters that we choose. One interesting feature of G is that it is not always positive. A negative G means that the atomic system alone is passive, indicating that the oscillation of the cavity mode is effectively damped by the atom. On the contour line of $G = 0$ (white line) in Fig. 2(a), Ω_c satisfies the relation

$$\Omega_c = \mathscr{A}_0\sqrt{\frac{\Gamma_{23}n_c(\Gamma_{23}n_c + \Gamma_{31}n_h)}{n_h(\Gamma_{23} - \Gamma_{31}) - \Gamma_{23}n_c}}, \quad (10)$$

with $\mathscr{A}_0 = \sqrt{(\Gamma_{23} + \Gamma_{31} + 2\Gamma_{23}n_c + \Gamma_{31}n_h)}/2$. Note that the square root operation in Eq. (10) is valid only if

$$n_c < \frac{n_h(\Gamma_{23} - \Gamma_{13})}{\Gamma_{23}}. \quad (11)$$

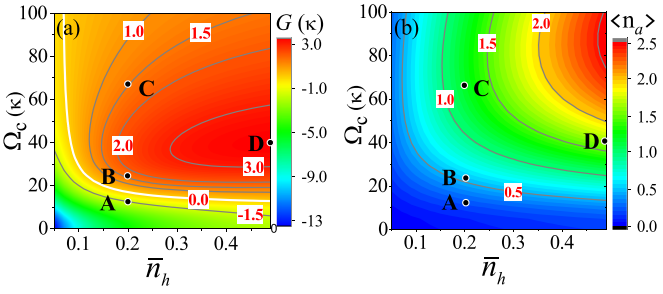

FIG. 2. (a) Lasing gain G with unit of κ obtained from Eq. (8) and (b) cavity photon number $\langle n_a\rangle$ obtained from Eq. (13) for different thermal occupation number of the hot reservoir and the Rabi frequency of the coupling field. $\Gamma_{13} = 32\,\kappa$, $\Gamma_{23} = 4\,\Gamma_{13}$, $\bar{n}_c = 0.05$, and $g_a = 35\,\kappa$. Black dots mark the particular points ($\bar{n}_h$, Ω_c) which are used in Fig. 3 for the photon number probability and Wigner function.

Thus one can assert that G would remain negative if the above condition is *not* satisfied. It tells us that in order to start the heat-engine process, one cannot use a cold bath having a higher energy density that could break the constraint of the condition (11). This is a quite natural result, especially from point of view of classical thermodynamics that a cooler tank is preferred when it is used as a cold reservoir.

Another even more interesting characteristic the condition (11) reveals is that the radiative decay rate of the transition $|3\rangle \leftrightarrow |2\rangle$ must be larger than that of $|3\rangle \leftrightarrow |1\rangle$, otherwise the system definitely remains passive. A similar property is found in the classical EIT engine, that only under the condition of $\Gamma_{23} \gg \Gamma_{13}$ can the relevant interaction be categorized as a heat-engine process from the angle of entropy; see the discussions in [30] on Eq. (8) and (10) therein.

III. PHOTON NUMBER STATISTICS

A classical description presented in the previous section provides a way to estimate the intensity of the output. A steady output of the engine suggests that $d\mathcal{E}/dt$ is zero, thus one can assert based on the expression in the parentheses in Eq. (7) that the intensity of the output electric field from the engine is proportional to $(G-\kappa)/(S\kappa)$. However, a more precise and rigorous description can be obtained only from a fully quantum description. Using the Fock basis $|n\rangle$ of the cavity mode, we can write the density operator ρ in Eq. (3) in a set of equations which take $\rho_{\alpha\beta;mn} = \langle\alpha, m|\rho|\beta, n\rangle$ as unknowns. Here $|\alpha\rangle, |\beta\rangle = |1\rangle, |2\rangle$ and $|3\rangle$, representing the energy levels of the atomic system, and $|m\rangle$, $|n\rangle = |0\rangle, |1\rangle, |2\rangle\cdots$ denoting the Fock states of the cavity mode:

$$\frac{d}{dt}\rho_{11;mn} = \mathscr{D}(\rho_{11;mn}) - \Gamma_h^+\rho_{11;mn} + \Gamma_h^-\rho_{33;mn} - ig_a(\sqrt{n}\rho_{13;m,n-1} - \sqrt{m}\rho_{31;m-1,n}), \quad (12a)$$

$$\frac{d}{dt}\rho_{22;mn} = \mathscr{D}(\rho_{22;mn}) - i\Omega_c\rho_{23;mn} + i\Omega_c^*\rho_{32;mn} - \Gamma_h^+\rho_{22;mn} + \Gamma_h^-\rho_{33;mn}, \quad (12b)$$

$$\frac{d}{dt}\rho_{33;mn} = \mathscr{D}(\rho_{33;mn}) + i\Omega_c\rho_{23;mn} - i\Omega_c^*\rho_{32;mn} - ig_a(\sqrt{n+1}\rho_{31;m,n+1} - \sqrt{m+1}\rho_{13;m+1,n}) + \Gamma_h^+\rho_{11;mn} - (\Gamma_h^- + \Gamma_c^-)\rho_{33;mn} + \Gamma_c^+\rho_{22;mn}, \quad (12c)$$

$$\frac{d}{dt}\rho_{32;mn} = \mathscr{D}(\rho_{32;mn}) - \gamma_{23}\rho_{32;mn} + i\Omega_c\rho_{22;mn} + ig_a\sqrt{m+1}\rho_{12;m+1,n} - i\Omega_c\rho_{33;mn}, \quad (12d)$$

$$\frac{d}{dt}\rho_{31;mn} = \mathscr{D}(\rho_{31;mn}) - \gamma_{13}\rho_{31;mn} + i\Omega_c\rho_{21;mn} - ig_a(\sqrt{n}\rho_{33;m,n-1} - \sqrt{m+1}\rho_{11;m+1,n}), \quad (12e)$$

$$\frac{d}{dt}\rho_{21;mn} = \mathscr{D}(\rho_{21;mn}) - \gamma_{12}\rho_{21;mn} + i\Omega_c^*\rho_{31;mn} - ig_a\sqrt{n}\rho_{23;m,n-1}. \quad (12f)$$

In the above equations, the term $\mathscr{D}(\rho_{\alpha\beta;mn})$ stands for the decays due to the cavity leaking, and $\mathscr{D}(\rho_{\alpha\beta;mn}) = -\frac{\kappa}{2}(m+n)\rho_{\alpha\beta;mn} + \kappa\sqrt{(m+1)(n+1)}\rho_{\alpha\beta;mn}$.

The state of the cavity mode is depicted by $\varrho = \mathrm{tr}_a(\rho)$ where tr_a represents the partial trace over the atomic space. Then the value of $P_n \equiv \varrho_{nn} = \rho_{11;nn} + \rho_{22;nn} + \rho_{33;nn}$ denotes the probability of finding n photons in such a cavity mode. Due to the presence of the classical coupling field, there are no single-excitation subspaces for these equations, and we have to solve them numerically. The results of P_n with the Fock states truncated at $n = 12$ are given as column (a) in Fig. 3. Through P_n, one can easily compute the cavity photon number

$$\langle\hat{n}_a\rangle = \sum_{n=0}^{\infty} nP_n. \quad (13)$$

Then using $\langle\hat{n}_a\rangle$ we plot the Poisson distribution $P_n^{\mathrm{Psn}} = e^{-\langle\hat{n}_a\rangle}\langle\hat{n}_a\rangle^n/n!$ and the thermal distribution $P_n^{\mathrm{Ther}} = \langle\hat{n}_a\rangle^n/(1+\langle\hat{n}_a\rangle)^{n+1}$ in the subfigures for comparison. If the distribution function becomes close to P_n^{Psn}, the output photons resemble the coherent light and the engine must be working far above the lasing threshold, otherwise it is similar to a thermal light source. In Fig. 3(a1) we set $\bar{n}_h = 0.2$, $\Omega_c = 12.5\,\kappa$ (point A in Fig. 2) and the corresponding gain parameter $G = -1.5\,\kappa$, meaning that the system is completely passive, and as we can see in Fig. 2(b), the brightness of the output (i.e., $\langle\hat{n}_a\rangle$) is approximately 0.26, and the photon number distribution looks like a thermal one, although the Poisson and thermal distributions are very similar to each other at lower $\langle\hat{n}_a\rangle$.

Fixing $\bar{n}_h$ at 0.2 and increasing Ω_c to $23.6\,\kappa$ and $66.3\,\kappa$ lead to the results in Figs. 3(a2) and 3(a3), respectively. The gain parameters at these two points [see B and C in Fig. 2(a)] have the same value of $G = 1.5\,\kappa$. However, the photon distributions are quite different. The comparison reveals the most significant contrast between the classical and quantum results, and it is also shown vividly in Fig. 2(b) that the structures of G and $\langle\hat{n}_a\rangle$ are not exactly the same: $\langle\hat{n}_a\rangle$ at point C is clearly above unity while $\langle\hat{n}_a\rangle$ at point B is lower.

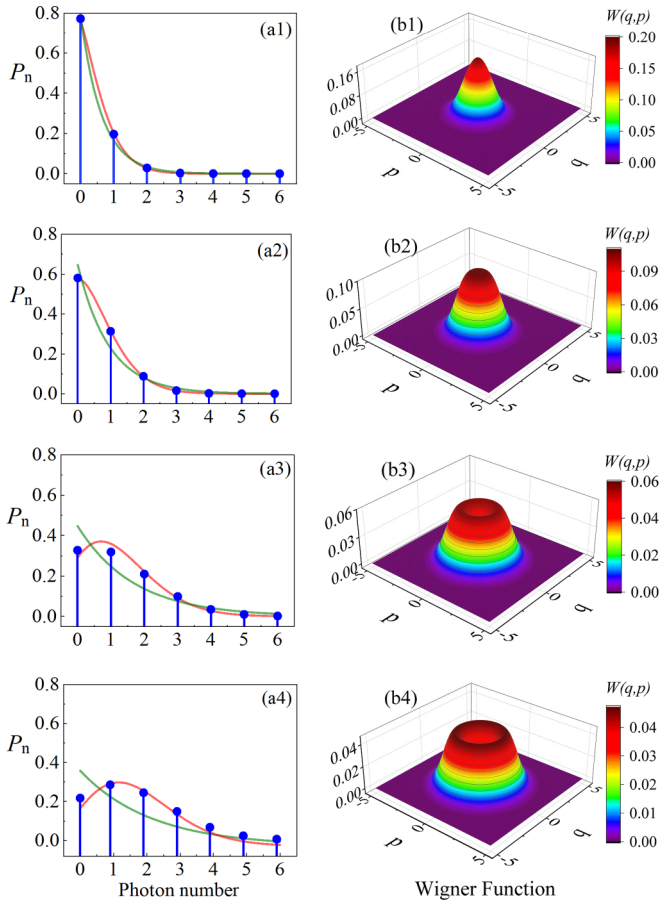

FIG. 3. Photon number probability $P(n)$ (blue dots) for (a1) $\bar{n}_h = 0.2$, $\Omega_c = 12.5\,\kappa$, (a2) $\bar{n}_h = 0.2$, $\Omega_c = 23.6\,\kappa$, (a3) $\bar{n}_h = 0.2$, $\Omega_c = 66.3\,\kappa$, (a4) $\bar{n}_h = 0.5$, $\Omega_c = 40.0\,\kappa$. The gain parameter $G = -1.5\,\kappa$ in (a1), and it takes the same value of $1.5\,\kappa$ in (a2) and (a3). $G = 3.5\kappa$ in (a4). The red (green) line is the Poisson (thermal) distribution with the same mean photon number $\langle n_a\rangle$. The other parameters are $\Gamma_{13} = 32\,\kappa$, $\Gamma_{23} = 4\,\Gamma_{13}$, $\bar{n}_c = 0.05$, and $g = 35\,\kappa$. The corresponding Wigner functions are given, respectively, as column (b).

We also manage to find the maximal value of G in Fig. 2(a), which corresponds to point D. The averaged photon number $\langle\hat{n}_a\rangle$ reaches 1.8, and the resultant photon distribution is plotted in Fig. 3(a4). Again one can clearly notice that the point of the maximal value of G does not corresponds to that of $\langle\hat{n}_a\rangle$ in the $\bar{n}_h$-Ω_c plane. Similar to the result of Fig. 3(a3), the photon distribution in (a4) is very close to the Poisson distribution, indicating that the system is about to generate a laser.

The Wigner function $W(q, p)$ is calculated from the reduced density matrix $\hat{\varrho}$. The results are presented as column (b) in Fig. 3. With the part of atom traced out, $\hat{\varrho}$ manifests itself as a diagonal matrix in the Fock basis. The corresponding Wigner function is centrosymmetric with respect to the origin. For the lower $\langle\hat{n}_a\rangle$ as shown in Figs. 3(b1) and 3(b2), the Wigner function is a single peak at origin indicating the system is not oscillating. As $\langle\hat{n}_a\rangle$ get larger [see Figs. 3(b3) and 3(b4)] a dip appears at the origin, and the overall structure of the Wigner function resembles a phase diagram of a classical harmonic oscillator with constant energy.

IV. THERMODYNAMICS OF THE ENGINE

The performance of the engine is normally characterized by the power and efficiency, which in turn relate to the first and second law of thermodynamics. In this section we investigate what the laws of thermodynamics look like in such a single-atom engine and show the features of its performance.

The first law of the thermodynamics can be examined from the the energy of the unperturbed atomic system, that is, $\hat{H}_0 = \sum_{i=1}^{3} \hbar\omega_i |i\rangle\langle i|$, with ω_i being the eigenfrequency of the corresponding atomic level. Considering that the operator $\hat{H}_0$ does not depend on time, then the changing rate of such energy $E = \mathrm{tr}(\rho\hat{H}_0)$ with respect to time is

$$\frac{dE}{dt} = \mathrm{tr}\left(\frac{\partial\rho}{\partial t}\hat{H}_0\right). \tag{14}$$

Substituting Eq. (3) into the above equation we have

$$\frac{dE}{dt} = P_c - \dot{Q}_{\mathrm{out}} + \dot{Q}_h - \dot{Q}_c. \tag{15}$$

The positive sign (prefactor signs in the above equation) means that energy transfers into the system. P_c and $\dot{Q}_{\mathrm{out}}$ result from the first term on the right-hand side of the master equation (3): $-\frac{i}{\hbar}\mathrm{tr}\{[H_0, V]\rho\} = P_c - \dot{Q}_{\mathrm{out}}$, with

$$P_c = i\hbar\omega_{32}\Omega_c(\langle\hat{\sigma}_{32}\rangle - \mathrm{H.c.}), \tag{16a}$$

$$\dot{Q}_{\mathrm{out}} = i\hbar\omega_{31}g_a(\langle\hat{\sigma}_{13}a^\dagger\rangle - \mathrm{H.c.}). \tag{16b}$$

P_c represents the energy per second that the system absorbs from the coupling field, and $\dot{Q}_{\mathrm{out}}$ is the power of the engine's output. The hot reservoir provides the energy at the rate

$$\begin{aligned}\dot{Q}_h &= \mathrm{tr}\{\mathscr{L}_h(\rho)\hat{H}_0\} \\ &= \hbar\omega_{31}\Gamma_{13}[\bar{n}_h\langle\hat{\sigma}_{11}\rangle - (\bar{n}_h+1)\langle\hat{\sigma}_{33}\rangle].\end{aligned} \tag{16c}$$

The waste energy is transferred into the cold reservoir at the rate

$$\begin{aligned}\dot{Q}_c &= -\mathrm{tr}\{\mathscr{L}_c(\rho)\hat{H}_0\} \\ &= \hbar\omega_{32}\Gamma_{23}[(\bar{n}_c+1)\langle\hat{\sigma}_{33}\rangle - \bar{n}_c\langle\hat{\sigma}_{22}\rangle].\end{aligned} \tag{16d}$$

Using the above definitions, the quantities P_c, $\dot{Q}_h$, $\dot{Q}_c$, and $\dot{Q}_{\mathrm{out}}$ are all positive when the heat-engine process dominates the interaction between the light and atom. Comparing the result (16b) and (16c) with Eq. (5a) we find that in the steady state ($d\langle\hat{\sigma}_{ij}\rangle/dt = 0$),

$$\dot{Q}_{\mathrm{out}} = \dot{Q}_h. \tag{17}$$

Additionally, Eq. (5b) suggests that

$$P_c = \dot{Q}_c. \tag{18}$$

Equations (17) and (18) indicate that the output energy of the engine is simply the energy taken from the hot bath. The flow of the energy is supported by the coherent coupling field, and the energy absorbed from which is exactly the amount used by the engine to compensate for the energy dumped into the cold bath. Note that whether the semiclassical approximation is adopted or not, the relations always hold. Overall, the energy that goes into the atomic system is equal to the energy that goes out ($dE/dt = 0$), which is the first law of thermodynamics.

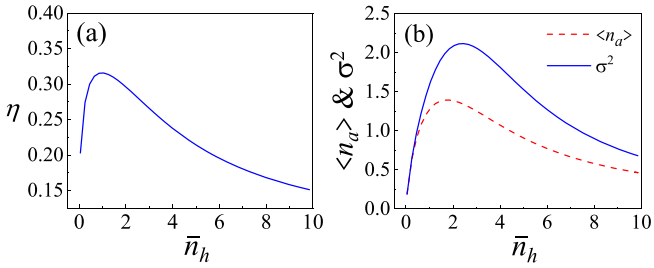

FIG. 4. Efficiency η (a), average photon number $\langle\hat{n}_a\rangle$ [red line in (b)], and variance σ^2 [blue line in (b)] plotted against thermal occupation number of the hot bath. Other parameters are $\Gamma_{13} = 32\kappa$, $\Gamma_{23} = 4\Gamma_{13}$, $\bar{n}_c = 0.05$, and $g = 35\kappa$.

We can also inspect the balance of engine through the energy of the output photons $E_a = \mathrm{tr}(\rho\hat{H}_a)$ with $\hat{H}_a$ being the free Hamiltonian of the cavity mode $\hat{H}_a = \hbar\omega_{31}\hat{a}^\dagger\hat{a}$. Similarly to the atomic part, $dE_a/dt = \mathrm{tr}(\frac{\partial\rho}{\partial t}\hat{H}_a)$ is composed of two part as well. The first part is the energy converted into photons per second by the engine $-\frac{i}{\hbar}\mathrm{tr}\{[H_a, V]\rho\}$, which is $i\hbar\omega_{31}g[\langle\hat{\sigma}_{13}a^\dagger\rangle - \mathrm{H.c.}]$. Note that this is just $\dot{Q}_{\mathrm{out}}$ in Eq. (16b). The second part is the energy leaking out of an optical cavity at the rate of $\mathrm{tr}\{\mathscr{L}_{\mathrm{cav}}(\rho)\hat{H}_a\}$, which is $-\hbar\omega_{31}\kappa\langle\hat{n}_a\rangle$. Using the last equation in Eq. (5) we can write the dynamics of the brightness as

$$\frac{\partial\langle\hat{n}_a\rangle}{\partial t} = -\kappa\langle\hat{n}_a\rangle + ig[\langle\hat{\sigma}_{13}a^\dagger\rangle - \mathrm{H.c.}]. \tag{19}$$

Then the steady-state condition $\partial\langle\hat{n}_a\rangle/\partial t = 0$ indicates that these two parts cancel each other and lead to the balance of energy in the generated field. Finally, the output power of the engine can be written in terms of the brightness as

$$\dot{Q}_{\mathrm{out}} = \hbar\omega_{31}\kappa\langle\hat{n}_a\rangle. \tag{20}$$

The engine is powered by the hot reservoir and the coupling field; then the efficiency of the system can be written as

$$\eta = \frac{\dot{Q}_{\mathrm{out}}}{\dot{Q}_h + P_c} = \frac{\dot{Q}_h}{\dot{Q}_h + \dot{Q}_c}, \tag{21}$$

if the relations (17) and (18) are considered.

The efficiency depends on how the engine is powered. Figure 4(a) shows that η increases as $\bar{n}_h$ gets larger, and after it passes a certain value, the efficiency begins to drop. This is mainly because the decoherence rate between the ground levels increases with the thermal occupation numbers of the thermal bath [see Eq. (6)]. The higher temperature of the hot bath makes the atomic coherence fade more quickly and consequently reduces the efficiency.

The second law of thermodynamics allows us to get a clear picture of the maximal efficiency of the system. As we can see, the engine system is composed of five parts, which are the hot and cold baths, the coupling field, the generated photons, and the cavity (including the atom). Let us assume that the entropy of the cavity is S, then the entropy production function is [6]

$$\delta = \frac{dS}{dt} - \frac{\dot{Q}_h}{\mathscr{T}_h} + \frac{\dot{Q}_c}{\mathscr{T}_c} + \frac{\dot{Q}_{\mathrm{out}}}{\mathscr{T}_{\mathrm{out}}}, \tag{22}$$

where we use $\mathscr{T}_\alpha$ with $\alpha \in \{h, c, \mathrm{out}\}$ to represent the flux temperature of the corresponding radiation. The reciprocal

of flux temperature is the entropy flow rate per unit power [34,35]. For the hot and cold baths assumed as black-body radiations, $\mathscr{T}_\alpha = \frac{3}{4}T_\alpha$ with $\alpha \in \{h, c\}$. The derivation in detail about this relation can be found in Ref. [36]. Since the classical coupling field is assumed to be an ideal laser with flux temperature approaching infinity, absorbing photons from it does not change the entropy of the whole system. Considering the cavity always returns to its initial state for each generated photon, thus $dS/dt = 0$. Then according to the second law of thermodynamics, the total entropy change of such a closed system must be greater than or equal to zero:

$$-\frac{\dot{Q}_h}{\mathscr{T}_h} + \frac{\dot{Q}_c}{\mathscr{T}_c} + \frac{\dot{Q}_{\text{out}}}{\mathscr{T}_{\text{out}}} \geqslant 0. \tag{23}$$

If we further assume that the system is far above the threshold of lasing, $\mathscr{T}_{\text{out}}$ will approach infinity as well. Together with Eq. (21), we find the maximal efficiency is

$$\eta_{\max} = \frac{\mathscr{T}_h}{\mathscr{T}_c + \mathscr{T}_h}. \tag{24}$$

This actually is the efficiency of the atomic-ensemble based EIT heat engine proposed by Harris, and it is far above that of the single-atom system we discuss in this paper.

We present the average photon number $\langle \hat{n}_a \rangle$ and the variance $\sigma^2 = \langle \hat{n}_a^2 \rangle - \langle \hat{n}_a \rangle^2$ in Fig. 4(b). Similar to the efficiency, the average photon number, which is also the power of the engine, and the variance both increase first with the increasing $\bar{n}_h$ and then decrease. But the variance is always larger than the average photon number, indicating that the statistics of the generated photon is super-Poissonian. In a realistic laser system there are more than one atom in the cavity. With N being the number of atoms, the coupling strength is effectively enhanced by $\sqrt{N}$ times. Then one would expect a Poisson distribution and efficiency approaching Eq. (24).

The vanishing entropy suggests that the energy coming from the coupling field should be considered as (input) work [13,36]. The energy of the generated photons is the output work if the engine is lasing. Then we can change our perspective on efficiency by considering that the output work is the amplification of the input work, with a "net" efficiency:

$$\eta_{\text{net}} = \frac{\dot{Q}_{\text{out}} - P_c}{\dot{Q}_h} = \frac{\dot{Q}_h - \dot{Q}_c}{\dot{Q}_h} = 1 - \frac{\mathscr{T}_c}{\mathscr{T}_h}, \tag{25}$$

which is the Carnot efficiency showing the maximal attainable amount of work we can extract (as the amount of increment) from the heat bath.

V. SUMMARY

We have investigated a single-atom version of the quantum heat engine based on electromagnetically induced transparency. Using both the semiclassical and full quantum approaches we showed the dependence of the classical gain and power of the engine on the thermal occupation number and the Rabi frequency of the coupling field. Calculations suggest that the difference choices of hot-bath temperatures and coupling Rabi frequencies can lead to the same classical gain, but different quantum statistics of the output photons. In our calculation, values of the parameters having a unit of frequency, such as the Rabi frequencies and the decay rates, are given as multiples of the cavity-loss rate, forming the conclusions; e.g., quantum statistics shown in Fig. 3 do not depend on a particular choice of the cavity-loss rate. When the temperature of the hot bath is relatively low, it appears that the power of the engine increases with it. But relatively strong pumping of the hot bath leads to poor performance of the engine due to the fact that the effect of EIT is also weakened by such incoherent coupling. When the first and second law of thermodynamics are applied to the engine process we found that the power of the output is simply the energy per time absorbed from the hot reservoir, and the energy released to the cold reservoir comes from the coupling field. If the engine is operated far above the threshold of lasing, then the entropy balance of the system suggests that the efficiency of the engine depends only on the temperature of the hot and cold bath, which resembles the original model using an atomic ensemble.

ACKNOWLEDGMENTS

We would like to thank the anonymous reviewer, whose comments on this paper significantly improved the quality of our discussion. The work is supported by the National Natural Science Foundation of China (Grants No. 12074061, No. 12274064, and No. 62375047) and Natural Science Foundation of Jilin Province (subject arrangement project) under Grant No. 20210101406JC.

[1] H. E. D. Scovil and E. O. Schulz-DuBois, Three-level masers as heat engines, Phys. Rev. Lett. **2**, 262 (1959).
[2] R. Kosloff, Quantum thermodynamics: A dynamical viewpoint, Entropy **15**, 2100 (2013).
[3] S. Vinjanampathy and J. Anders, Quantum thermodynamics, Contemp. Phys. **57**, 545 (2016).
[4] H. T. Quan, Y.-X. Liu, C. P. Sun, and F. Nori, Quantum thermodynamic cycles and quantum heat engines, Phys. Rev. E **76**, 031105 (2007).
[5] R. Alicki, The quantum open system as a model of the heat engine, J. Phys. A **12**, L103 (1979).
[6] H. Spohn, Entropy production for quantum dynamical semigroups, J. Math. Phys. **19**, 1227 (1978).
[7] E. Boukobza and D. J. Tannor, Thermodynamics of bipartite systems: Application to light-matter interactions, Phys. Rev. A **74**, 063823 (2006).
[8] M. Qutubuddin and K. E. Dorfman, Incoherent control of optical signals: Quantum-heat-engine approach, Phys. Rev. Res. **3**, 023029 (2021).
[9] K. Beyer, K. Luoma, and W. T. Strunz, Steering heat engines: A truly quantum Maxwell demon, Phys. Rev. Lett. **123**, 250606 (2019).
[10] A. Hewgill, A. Ferraro, and G. De Chiara, Quantum correlations and thermodynamic performances of two-qubit engines with local and common baths, Phys. Rev. A **98**, 042102 (2018).

[11] A. E. Allahverdyan and T. M. Nieuwenhuizen, Breakdown of the Landauer bound for information erasure in the quantum regime, Phys. Rev. E **64**, 056117 (2001).
[12] L. del Rio, J. Aberg, R. Renner, O. Dahlsten, and V. Vedral, The thermodynamic meaning of negative entropy, Nature (London) **474**, 61 (2011).
[13] M. O. Scully, M. S. Zubairy, G. S. Agarwal, and H. Walther, Extracting work from a single heat bath via vanishing quantum coherence, Science **299**, 862 (2003).
[14] P. A. Camati, J. F. G. Santos, and R. M. Serra, Coherence effects in the performance of the quantum Otto heat engine, Phys. Rev. A **99**, 062103 (2019).
[15] M. O. Scully, Quantum photocell: Using quantum coherence to reduce radiative recombination and increase efficiency, Phys. Rev. Lett. **104**, 207701 (2010).
[16] J. M. Diaz de la Cruz and M. A. Martin-Delgado, Quantum-information engines with many-body states attaining optimal extractable work with quantum control, Phys. Rev. A **89**, 032327 (2014).
[17] M. Campisi, J. Pekola, and R. Fazio, Nonequilibrium fluctuations in quantum heat engines: Theory, example, and possible solid state experiments, New J. Phys. **17**, 035012 (2015).
[18] G. Watanabe, B. P. Venkatesh, P. Talkner, M.-J. Hwang, and A. del Campo, Quantum statistical enhancement of the collective performance of multiple bosonic engines, Phys. Rev. Lett. **124**, 210603 (2020).
[19] N. M. Myers and S. Deffner, Bosons outperform fermions: The thermodynamic advantage of symmetry, Phys. Rev. E **101**, 012110 (2020).
[20] E. Geva and R. Kosloff, A quantum-mechanical heat engine operating in finite time. A model consisting of spin-1/2 systems as the working fluid, J. Chem. Phys. **96**, 3054 (1992).
[21] R. Kosloff and T. Feldmann, Discrete four-stroke quantum heat engine exploring the origin of friction, Phys. Rev. E **65**, 055102(R) (2002).
[22] T. D. Kieu, The second law, Maxwell's demon, and work derivable from quantum heat engines, Phys. Rev. Lett. **93**, 140403 (2004).
[23] N. Linden, S. Popescu, and P. Skrzypczyk, How small can thermal machines be? The smallest possible refrigerator, Phys. Rev. Lett. **105**, 130401 (2010).
[24] M. P. Müller, Correlating thermal machines and the second law at the nanoscale, Phys. Rev. X **8**, 041051 (2018).
[25] G. D. Chiara, G. Landi, A. Hewgill, B. Reid, A. Ferraro, A. J. Roncaglia, and M. Antezza, Reconciliation of quantum local master equations with thermodynamics, New J. Phys. **20**, 113024 (2018).
[26] F. Clivaz, R. Silva, G. Haack, J. B. Brask, N. Brunner, and M. Huber, Unifying paradigms of quantum refrigeration: A universal and attainable bound on cooling, Phys. Rev. Lett. **123**, 170605 (2019).
[27] J. Roßnagel, O. Abah, F. Schmidt-Kaler, K. Singer, and E. Lutz, Nanoscale heat engine beyond the Carnot limit, Phys. Rev. Lett. **112**, 030602 (2014).
[28] K. Ptaszyński, Non-Markovian thermal operations boosting the performance of quantum heat engines, Phys. Rev. E **106**, 014114 (2022).
[29] J.-F. Chen, C.-P. Sun, and H. Dong, Achieve higher efficiency at maximum power with finite-time quantum Otto cycle, Phys. Rev. E **100**, 062140 (2019).
[30] S. E. Harris, Electromagnetically induced transparency and quantum heat engines, Phys. Rev. A **94**, 053859 (2016).
[31] M. Fleischhauer, A. Imamoglu, and J. P. Marangos, Electromagnetically induced transparency: Optics in coherent media, Rev. Mod. Phys. **77**, 633 (2005).
[32] Y. Zou, Y. Jiang, Y. Mei, X. Guo, and S. Du, Quantum heat engine using electromagnetically induced transparency, Phys. Rev. Lett. **119**, 050602 (2017).
[33] S.-W. Li, M. B. Kim, G. S. Agarwal, and M. O. Scully, Quantum statistics of a single-atom Scovil–Schulz-DuBois heat engine, Phys. Rev. A **96**, 063806 (2017).
[34] X. L. Ruan, S. C. Rand, and M. Kaviany, Entropy and efficiency in laser cooling of solids, Phys. Rev. B **75**, 214304 (2007).
[35] L. D. Landau, On the thermodynamics of photoluminescence, in *Collected Papers of L. D. Landau*, edited by D. T. Haar (Pergamon, New York, 1965), pp. 461–465.
[36] C. E. Mungan, Radiation thermodynamics with applications to lasing and fluorescent cooling, Am. J. Phys. **73**, 315 (2005).